International Journal of Thermophysics (2024) 45:61
https://doi.org/10.1007/s10765-024-03351-1

Fourier Transform Thermoreflectance Method Under Front-Heat Front-Detect Configuration

Takahiro Baba[1,2] · Tetsuya Baba[1] · Takao Mori[1,2]

Received: 8 January 2024 / Accepted: 20 February 2024
© The Author(s) 2024

Abstract

The thermoreflectance method, which can measure thermal diffusivity in the cross-plane direction of thin films, mainly has two possible configurations; rear-heat front-detect (RF) and front-heat front-detect (FF) configuration. FF configuration is applicable to a wide variety of thin films including thin films deposited on opaque substrates, but this configuration has some problems in determination of the thermal diffusivity. One of the main problems is the effect of the penetration of pump beam and probe beam in thin film, which affects the initial temperature distribution near the sample's surface after pulse heating. Several studies have tried to analyze the effect but there have been no practical analytical solutions which can solve this problem in FF configuration. In this paper, we propose a new analytical solution which considers the penetration of pump beam and probe beam into thin film, and by applying Fourier expansion analysis which we developed in a previous study to thermoreflectance signals, we have determined the thermal diffusivity of thin film in the thermoreflectance method under FF configuration. We measured platinum thin films with different thickness under both FF and RF configuration and obtained consistent thermal diffusivity values from both configurations.

Keywords Fourier transform · Penetration of pump beam and probe beam · Thermal diffusivity · Thermoreflectance · Thin film

✉ Takao Mori
MORI.Takao@nims.go.jp

[1] Research Center for Materials Nanoarchitectonics (MANA), National Institute for Materials Science (NIMS), Namiki 1-1, Tsukuba, Ibaraki 305-0044, Japan

[2] Graduate School of Pure and Applied Science, University of Tsukuba, Tennoudai 1-1-1, Tsukuba, Ibaraki 305-8671, Japan

Published online: 25 March 2024

1 Introduction

Reliable thermophysical property values of thin films are important to develop advanced electronics devices such as highly integrated electronic devices, phase-change memories, magneto-optical disks, light-emitting diodes (LEDs), and semiconductor lasers (LDs) [1–5]. Semiconductor devices such as central processing unit (CPU) are composed of thin films and thin wires with a scale much smaller than 100 nm. Since the temperature of semiconductor devices is raised by Joule heating of electric current under operation, it is primarily important to understand the flow of heat inside the device and perform thermal design to improve the degree of integration and clock speed thereby suppressing overheating of the device. In recording media such as DVD-RAM and Phase-change memory, recording is performed by heating a minute area with a laser beam or electric current and changing the state of that area (magnetization, crystalline phase, and amorphous phase) [6]. The key technology is controlling temperature changes inside the recording medium using pulse heating. Furthermore, in the development of novel thermoelectric thin films, thermal conductivity or thermal diffusivity is one of the key properties to evaluate non-dimensional figure of merit of the material [7, 8].

The picosecond thermoreflectance method was invented by Paddock and Eesley for measuring thermal diffusivity of thin films [9]. Different wavelengths of dye lasers excited by a mode-locked argon ion laser were used as pump beam and probe beam. Since reflectivity of material surface varies depending on the surface temperature, a change of the sample's front surface temperature can be observed by a change of reflected light intensity detected by photodiode. This temperature measurement method gauged via the temperature change of reflectivity is called the thermoreflectance method [10]. This method was applied, for example, to measure cross-plane thermal diffusivity of aluminum thin films from 50 nm, 100 nm, and 500 nm thick by the National Research Laboratory of Metrology [11–13].

However, these studies by the picosecond thermoreflectance measurement under front-heat front-detect (FF) configuration were less successful to determine cross-plane thermal diffusivity of thin films, compared to the flash method for bulk materials [14–17], because of the following reasons.

1. Since the pulse interval of pump beam was as short as 13 ns, the influence of heating from previous pulses is large. Therefore, it is difficult to quantitatively analyze the signal using the heat diffusion equation.
2. Since the delay time between pump beam and probe beam was typically controlled by using optical delay lines, the observation time was shorter than 6 ns which is smaller than the pulse interval of 13 ns.
3. The pump beam does not heat just the surface of the sample since the beam penetrates into the thin film and exponentially decays from the surface with an attenuation length of 10 nm order. This is also the case for the probe beam. Although these effects were analyzed [18, 19], an analytical equation considering the penetration of both pump beam and probe beam has not been obtained.

To avoid these disadvantages of picosecond thermoreflectance method under FF configuration, the National Research Laboratory of Metrology shifted its research focus from FF configuration to rear-heat front-detect (RF) configuration, which are geometrically similar to the flash method [20–23]. This approach has been successful to measure the cross-plane thermal diffusivity of thin films with the same reliability as the flash method. However, although a thin metallic film on a transparent substrate can be measured under RF configuration, thin films on opaque substrate could not be measured under this configuration.

To meet the urgent needs of material science and technology, an engineering approach was introduced to the picosecond thermoreflectance method under FF configuration, where thermal diffusivity and thermal conductivity of the first layer, which is called as the transducer by this approach, are approximated to be infinitely large. Then, the thermophysical properties of the second and subsequent layers are estimated by analyzing the cooling curve of the surface of the first layer under the FF configuration [24–26]. Now the term "Time Domain Thermoreflectance (TDTR) method" is often used for this specific approach to derive thermal diffusivity values from thermoreflectance signals in time domain. Many studies by the TDTR method have been reported including temperature-dependent thermal boundary conductance at Al_2O_3 and Pt/Al_2O_3 interfaces [27] and simultaneous measurement of thermal conductivity and specific heat capacity [28].

The National Research Laboratory of Metrology was reorganized to the National Metrology Institute of Japan (NMIJ) in 2001. Key technologies have been developed in NMIJ to solve the two constraints of picosecond thermoreflectance measurements, 1. 2. mentioned above. First one is control of delay time between pump beam and probe beam, using electrical control by Taketoshi et al. [29]. This technology realized measurement of thermoreflectance signal over the entire period of pulse interval. Second one is replacement of "Ti–Sapphire lasers with pulse interval of 13 ns" to "mode-locked fiber laser with a pulse interval of 50 ns" by Yagi et al. [23, 30, 31]. This technology enabled to observe thermoreflectance signals over the entire period of 50 ns. By replacing the large-scale and expensive Ti–sapphire laser system with the compact fiber-laser system, this measuring instrument can be assembled much more compactly, cost-effective, and enable it to be popularized for wide use by science and technology.

Recently, a new analytical approach based on Fourier transform, which can reproduce temperature responses over the entire range of pulse interval, was developed by Baba et al. [32]. This analytical approach has reduced the uncertainty of thermal diffusivity determination by the thermoreflectance method under RF configuration. This approach has also been extended to simultaneously determine thermal diffusivity of thin film and interfacial thermal resistance between thin film and substrate [33].

In this study, we report the application of the Fourier transform approach to the thermoreflectance method under the FF configuration.

2 Experiments

Figure 1 shows a schematic diagram of the thermoreflectance method in front-heat front-detect (FF) configuration. In the case of FF configuration, a laser beam is incident on the surface of thin film to heat up the surface. Another laser beam is incident on the same surface and reflection from the surface is detected by photodetector to observe the surface temperature. The wavelength of pump beam and probe beam are 1550 nm and 775 nm, respectively. More detailed information about our experimental setup is explained in our previous work [32].

In actual thermoreflectance measurements, heat transfer across thin films can be regarded as one-dimensional because diameter of the pump beam, which is 45 µm in our apparatus, is far larger than thickness of thin films. Thus, analytical solutions for temperature responses from a sample can be derived from one-dimensional heat equation.

3 Analysis

3.1 Heat Diffusion Across Thin Film on Substrate

If a sample is assumed to be a single-layered film on semi-infinite substrate as shown in Fig. 1, the relationship between the temperature at front surface of thin film T_f, the temperature at interface between thin film and substrate T_s, the heat flux across surface of thin film q_f , and the heat flux across the interface q_s is expressed as follows in Laplace domain [34]

$$\begin{bmatrix} \tilde{q}_s(\xi) \\ \tilde{T}_s(\xi) \end{bmatrix} = \begin{bmatrix} \cosh\left(\sqrt{\tau_f \xi}\right) & -b_f\sqrt{\xi}\sinh\left(\sqrt{\tau_f \xi}\right) \\ -\frac{1}{b_f\sqrt{\xi}}\sinh\left(\sqrt{\tau_f \xi}\right) & \cosh\left(\sqrt{\tau_f \xi}\right) \end{bmatrix} \begin{bmatrix} \tilde{q}_f(\xi) \\ \tilde{T}_f(\xi) \end{bmatrix} \tag{1}$$

$$\tau_f = \frac{{d_f}^2}{\alpha_f}, \tag{2}$$

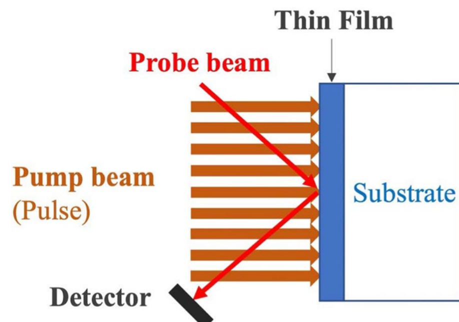

Fig. 1 Diagram of thermoreflectance method under front-heat front-detect (FF) configuration

where τ_f is heat diffusion time across thin film, d_f is thickness of thin film, α_f is thermal diffusivity of thin film, and b_f is thermal effusivity of thin film. ξ is a complex variable in Laplace domain.

When thickness of substrate is assumed to be semi-infinite, the temperature of the interface between thin film and substrate $\widetilde{T}_s(\xi)$ in Laplace transform is expressed as follows [34]

$$\widetilde{T}_s(\xi) = \frac{1}{b_s\sqrt{\xi}} \times \widetilde{q}_s(\xi), \tag{3}$$

where b_s is the thermal effusivity of substrate.

3.2 Effect of Penetration of Pump Beam

If a laser beam is incident on an actual material, the initial distribution of heat in the material can be expressed as follows

$$Q_i(x) = \kappa \exp(-\kappa x), \tag{4}$$

where κ is absorption coefficient, which is the reciprocal of penetration depth l. In the case of a semi-infinite material, the surface temperature of the material after pulse heating at distance x can be expressed as following Green's function [34].

$$G(x,t) = \frac{1}{b\sqrt{\pi t}} \times \exp\left(-\frac{x^2}{4\alpha t}\right), \tag{5}$$

where b is thermal effusivity and α is thermal diffusivity of material. The surface temperature of the material $T_f(t)$ can be expressed by the convolution of Eqs. 4 and 5 as follows

$$T_f(t) = \int_0^\infty G(x,t)Q_i(x)dx = \frac{2}{\sqrt{\pi}c\rho l}\exp\left(\frac{t}{\tau_i}\right)\mathrm{erfc}\left(\sqrt{\frac{t}{\tau_i}}\right) \tag{6}$$

$$\tau_i = \frac{l^2}{\alpha}, \tag{7}$$

where τ_i is heat diffusion time across the penetration depth, which means the heat diffusion time across the material whose thickness is the same as the penetration depth l.

3.3 Matrix Representation of Beam Penetration

Effect of beam penetration can be represented by a matrix as explained in this subchapter. The relationship between the temperature at front surface of thin film T_f, the temperature at interface between thin film and substrate T_s, the heat flux across surface of thin film q_f , and the heat flux across interface q_s is expressed as Eq. 1. If

the first layer has finite heat capacity and infinite thermal conductivity, Eq. 1 can be expressed as follows

$$\begin{bmatrix} \widetilde{q_s}(\xi) \\ \widetilde{T_s}(\xi) \end{bmatrix} = \begin{bmatrix} 1 & -C_f\xi \\ 0 & 1 \end{bmatrix} \begin{bmatrix} \widetilde{q_f}(\xi) \\ \widetilde{T_f}(\xi) \end{bmatrix} \tag{8}$$

$$C_f = c_f \rho_f d_f, \tag{9}$$

where C_f is heat capacity per unit area of thin film, c_f is specific heat capacity of thin film, and ρ_f is density of thin film. Considering Eq. 3 and $\widetilde{q_f}(\xi) = 1$, the Laplace transform of surface temperature $\widetilde{T_f}(\xi)$ can be expressed as follows:

$$\widetilde{T_f}(\xi) = \frac{1}{b_s\sqrt{\xi}} \times \frac{1}{1 + \sqrt{\tau_s \xi}} \tag{10}$$

$$\tau_s = \left(\frac{C_f}{b_s}\right)^2, \tag{11}$$

where τ_s is characteristic time called heat effusion time. The surface temperature $T_f(t)$ is expressed as inverse Laplace transform of $\widetilde{T_f}(\xi)$ as follows:

$$T_f(t) = \frac{2}{\sqrt{\pi} c_f \rho_f d_f} \exp\left(\frac{t}{\tau_s}\right) \mathrm{erfc}\left(\sqrt{\frac{t}{\tau_s}}\right) \tag{12}$$

Equation 12 is the same as Eq. 6 when $\tau_s = \tau_i$. This means penetration of laser beam can be regarded as heat effusion from a layer with finite heat capacity and infinite thermal conductivity since they are mathematically equivalent to each other.

An equation which considers the penetration of probe beam, as well as the penetration of pump beam, can be expressed by a linear combination of the above-mentioned equation with heat diffusion times associated with heating and detection, respectively (see Appendix for details). Therefore, the contribution from the penetration of both pump beam and probe beam can be expressed by the matrix in Eq. 8.

3.4 Effect of Beam Penetration into Thin Film on Substrate

To consider the contribution from the penetration of pump beam in thin film, we assumed that the thin film can be divided into two layers as shown in Fig. 2. The thickness of the first layer corresponds to the penetration depth of pump beam l. In this case, the temperature at the front end of the first layer is named $\widetilde{T_{f1}}(\xi)$ and the heat flux across the front end is named $\widetilde{q_{f1}}(\xi)$. On the other hand, the temperature at the interface between the first layer and second layer in thin film is named $\widetilde{T_{f2}}(\xi)$, which corresponds to the temperature at the front end of the second layer, and the

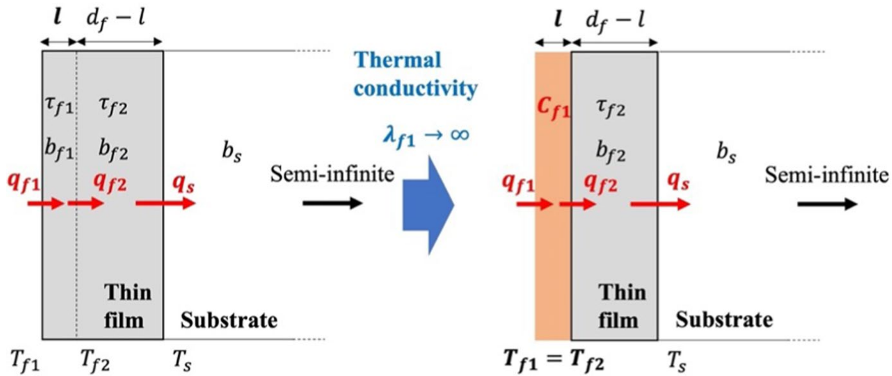

Fig. 2 Schematic diagram of two-layer (thin film and substrate) model with penetration of pump beam

heat flux across the interface is named $\widetilde{q_{f2}}(\xi)$. The relationship between temperature and heat flux can be extended by cascading quadrupole matrices as follows [34]

$$\begin{bmatrix} \widetilde{q_s}(\xi) \\ \widetilde{T_s}(\xi) \end{bmatrix} = \begin{bmatrix} \cosh\left(\sqrt{\tau_{f2}\xi}\right) & -b_{f2}\sqrt{\xi}\sinh\left(\sqrt{\tau_{f2}\xi}\right) \\ -\frac{1}{b_{f2}\sqrt{\xi}}\sinh\left(\sqrt{\tau_{f2}\xi}\right) & \cosh\left(\sqrt{\tau_{f2}\xi}\right) \end{bmatrix} \times \begin{bmatrix} \cosh\left(\sqrt{\tau_{f1}\xi}\right) & -b_{f1}\sqrt{\xi}\sinh\left(\sqrt{\tau_{f1}\xi}\right) \\ -\frac{1}{b_{f1}\sqrt{\xi}}\sinh\left(\sqrt{\tau_{f1}\xi}\right) & \cosh\left(\sqrt{\tau_{f1}\xi}\right) \end{bmatrix} \begin{bmatrix} \widetilde{q_{f1}}(\xi) \\ \widetilde{T_{f1}}(\xi) \end{bmatrix} \tag{13}$$

$$\tau_{f1} = \frac{l^2}{\alpha_{f1}} \tag{14}$$

$$\tau_{f2} = \frac{\left(d_f - l\right)^2}{\alpha_{f2}}, \tag{15}$$

where τ_{f1} is heat diffusion time across the first layer in thin film, τ_{f2} is heat diffusion time across the second layer in thin film, α_{f1} is thermal diffusivity of the first layer in thin film, α_{f2} is thermal diffusivity of the second layer in thin film, b_{f1} is thermal effusivity of the first layer in thin film, and b_{f2} is thermal effusivity of the second layer in thin film. If the first layer has finite heat capacity and infinite thermal conductivity λ_{f1} (i.e., infinite thermal diffusivity α_{f1}), each of the elements, which includes τ_{f1}, converges as follows:

$$\lim_{\alpha_{f1}\to\infty} \cosh\left(\sqrt{\tau_{f1}\xi}\right) = \lim_{\alpha_{f1}\to\infty} \cosh\left(\sqrt{\frac{l^2}{\alpha_{f1}}\xi}\right) = 1 \tag{16}$$

$$\lim_{\alpha_{f1}\to\infty}\frac{\sinh\left(\sqrt{\tau_{f1}\xi}\right)}{b_{f1}\sqrt{\xi}}=\lim_{\alpha_{f1}\to\infty}\frac{\sinh\left(\sqrt{\frac{l^2}{\alpha_{f1}}\xi}\right)}{c_f\rho_f\sqrt{\alpha_{f1}\xi}}=0 \tag{17}$$

$$\lim_{\alpha_{f1}\to\infty}b_{f1}\sqrt{\xi}\sinh\left(\sqrt{\tau_{f1}\xi}\right)=\lim_{\alpha_{f1}\to\infty}c_f\rho_f\sqrt{\alpha_{f1}\xi}\sinh\left(\sqrt{\frac{l^2}{\alpha_{f1}}\xi}\right)=C_{f1}\xi \tag{18}$$

$$C_{f1}=c_f\rho_f l, \tag{19}$$

where C_{f1} is heat capacity per unit area of the first layer in thin film. Therefore, Eq. 13 can be expressed as follows

$$\begin{bmatrix}\widetilde{q_s}(\xi)\\ \widetilde{T_s}(\xi)\end{bmatrix}=\begin{bmatrix}\cosh\left(\sqrt{\tau_{f2}\xi}\right) & -b_{f2}\sqrt{\xi}\sinh\left(\sqrt{\tau_{f2}\xi}\right)\\ -\frac{1}{b_{f2}\sqrt{\xi}}\sinh\left(\sqrt{\tau_{f2}\xi}\right) & \cosh\left(\sqrt{\tau_{f2}\xi}\right)\end{bmatrix}\begin{bmatrix}1 & -C_{f1}\xi\\ 0 & 1\end{bmatrix}\begin{bmatrix}\widetilde{q_{f1}}(\xi)\\ \widetilde{T_{f1}}(\xi)\end{bmatrix} \tag{20}$$

In thermoreflectance method, the surface of the thin film is assumed to be pulse heated, which can be expressed by Dirac delta function $\delta(t)$. The Laplace transform of $\delta(t)$ is 1. Considering Eq. 3 and $\widetilde{q_f}(\xi)=1$, the following relationship between heat flux and temperature can be obtained from Eq. 20.

$$b_s\sqrt{\xi}\widetilde{T_s}(\xi)=\cosh\left(\sqrt{\tau_{f2}\xi}\right)-\left(C_{f1}\xi\cosh\left(\sqrt{\tau_{f2}\xi}\right)+b_{f2}\sqrt{\xi}\sinh\left(\sqrt{\tau_{f2}\xi}\right)\right)\widetilde{T_{f1}}(\xi) \tag{21}$$

$$\widetilde{T_s}(\xi)=-\frac{1}{b_{f2}\sqrt{\xi}}\sinh\left(\sqrt{\tau_{f2}\xi}\right)+\left(\frac{C_{f1}}{b_{f2}}\sqrt{\xi}\sinh\left(\sqrt{\tau_{f2}\xi}\right)+\cosh\left(\sqrt{\tau_{f2}\xi}\right)\right)\widetilde{T_{f1}}(\xi) \tag{22}$$

By solving Eqs. 21 and 22, $\widetilde{T_{f1}}(\xi)$ is expressed as follows:

$$\widetilde{T_{f1}}(\xi)=\frac{1}{b_f\sqrt{\xi}}\times\frac{1+\gamma\exp\left(-2\sqrt{\tau_f\xi}\right)}{1-\gamma\exp\left(-2\sqrt{\tau_f\xi}\right)+\left(1+\gamma\exp\left(-2\sqrt{\tau_f\xi}\right)\right)\sqrt{\tau_i\xi}} \tag{23}$$

$$\tau_f=\frac{\left(d_f-l\right)^2}{\alpha_f} \tag{24}$$

$$\gamma=\frac{b_f-b_s}{b_f+b_s} \tag{25}$$

$$\tau_i=\left(\frac{C_{f1}}{b_f}\right)^2=\frac{l^2}{\alpha_f}, \tag{26}$$

where γ is non-dimensional parameter called ratio of virtual heat sources [34], and τ_i is heat diffusion time across the penetration depth. α_{f2}, τ_{f2} , and b_{f2} are replaced with α_f, τ_f , and b_f for convenience.

The surface temperature $\widetilde{T_{f1}}(\xi)$ can be regarded as proportional to the reflectance because actual temperature change in thermoreflectance method is small. Thus, the intensity of reflected probe beam can be expressed as follows:

$$\widetilde{Y}(\xi) = k\widetilde{T_{f1}}(\xi) = \frac{k}{b_f\sqrt{\xi}} \times \frac{1 + \gamma \exp\left(-2\sqrt{\tau_f \xi}\right)}{1 - \gamma \exp\left(-2\sqrt{\tau_f \xi}\right) + \left(1 + \gamma \exp\left(-2\sqrt{\tau_f \xi}\right)\right)\sqrt{\tau_i \xi}}, \tag{27}$$

where k is a proportionality constant. If the proportionality constant is redefined as $k\prime = k/b_f$, Eq. 27 can be expressed as follows

$$\widetilde{Y}(\xi) = \frac{k\prime}{b_f\sqrt{\xi}} \times \frac{1 + \gamma \exp\left(-2\sqrt{\tau_f \xi}\right)}{1 - \gamma \exp\left(-2\sqrt{\tau_f \xi}\right) + \left(1 + \gamma \exp\left(-2\sqrt{\tau_f \xi}\right)\right)\sqrt{\tau_i \xi}} \tag{28}$$

Equation 28, which expresses thermoreflectance signals, can be used as regression function in regression analysis. As we explained in the previous study, the regression analysis can be applied to Fourier coefficients of thermoreflectance signals in frequency domain [32].

4 Results

We measured platinum thin films (100 nm, 150 nm, and 200 nm thick) deposited on fused quartz substrate with a picosecond thermoreflectance apparatus PicoTR (NETZSCH-Gerätebau GmbH) under FF configuration. Figure 3(a), (b), and (c) shows thermoreflectance signals from 0 s to 5 ns, observed from the 100 nm thick, 150 nm thick, and 200 nm thick Pt thin film, respectively. The signals were sampled at 100 GHz sampling rate (10 ps sampling interval). The interval of periodic pulse of pump beam ΔT is 50 ns. Fourier coefficient Y_n was calculated from the thermoreflectance signal by using DFT in the range of 0 s to 50 ns [32]. After obtaining Y_n, least squares method was applied to the absolute value of the Fourier coefficient $|Y_n|$ as follows:

$$|Y_n| = |\widetilde{Y}(\nu_n, \widehat{k\prime}, \widehat{\tau_f}, \widehat{\gamma}, \widehat{\tau_i})| + \varepsilon, \tag{29}$$

where ν_n is frequency and ε is error. $\widehat{k\prime}$, $\widehat{\tau_f}$, $\widehat{\gamma}$, and $\widehat{\tau_i}$ are estimates of fitting parameters $k\prime$, τ_f, γ , and τ_i. By estimating fitting parameters, l, α_f, b_f , and b_s are determined by following equations.

$$l = \frac{1}{1 + \sqrt{\frac{\widehat{\tau_f}}{\widehat{\tau_i}}}} \times d_f \tag{30}$$

Fig. 3 (a): Thermoreflectance signal under FF configuration from the 100 nm thick Pt film and regression curves in time domain. (b): Thermoreflectance signal under FF configuration from the 150 nm thick Pt film and regression curves in time domain. (c): Thermoreflectance signal under FF configuration from the 200 nm thick Pt film and regression curves in time domain ▶

$$\alpha_f = \frac{\left(d_f - l\right)^2}{\hat{\tau}_f} \tag{31}$$

$$b_f = \sqrt{\alpha_f} c_f \rho_f \tag{32}$$

$$b_s = b_f \frac{1 - \hat{\gamma}}{1 + \hat{\gamma}} \tag{33}$$

Equation 30 is derived from Eqs. 24 and 26. Figure 4 shows the absolute value of the Fourier coefficient $|Y_n|$ obtained from the signal in Fig. 3(a) and the regression curve in frequency domain. Frequency components above 20 GHz, which are not significant, are discarded. Table 1 shows estimates of fitting parameters $\hat{\tau}_f$, $\hat{\gamma}$, and $\hat{\tau}_i$, obtained by applying least squares method to the absolutes of Fourier coefficients $|Y_n|$. Thermal diffusivity of thin film α_f and penetration depth of pump beam l were determined by the estimates of the fitting parameters. The specific heat capacity c_f and density ρ_f are $133\,\text{J} \cdot (\text{kg} \cdot \text{K})^{-1}$ and $21500\,\text{kg} \cdot \text{m}^{-3}$, respectively, which are literature values for platinum [35]. The red lines in Fig. 3 and 4 show regression curves derived from Eq. 28 in time domain and frequency domain, respectively. The regression curves, which are calculated by Fourier series, are oscillating at around 0 s because of Gibbs phenomenon. Figure 5 shows the thermoreflectance signal from the 100 nm thick Pt film and its regression curve in the whole observation time of 50 ns, which is zoomed in Fig. 3(a). By considering the contributions from τ_i, the regression curve can fit the signals in the whole observation time.

We measured each of the films three times under FF configuration, and under RF configuration as well. Figure 6 shows normalized thermoreflectance signals obtained from the 200 nm thick Pt film under both FF and RF configuration. Both signals close to each other after heat diffusion time of the film. Tables 2 and 3 show thermal diffusivity values and penetration depth values obtained from the whole measurement, respectively. Average values and standard deviations in three measurements were also calculated. The determination of thermal diffusivity of Pt thin film is consistent, and their relative values of standard deviation (SD/Average) are less than 10 % for the 100 nm thick and 150 nm thick Pt thin film. The values under FF configuration agree with these under RF configuration within smaller deviation than 10 % for 150 nm thick and 200 nm thick Pt thin film. The determination of penetration depth of pump beam is also consistent, and their relative values of standard deviation are less than 10 % for the 100 nm thick and 150 nm thick Pt thin film.

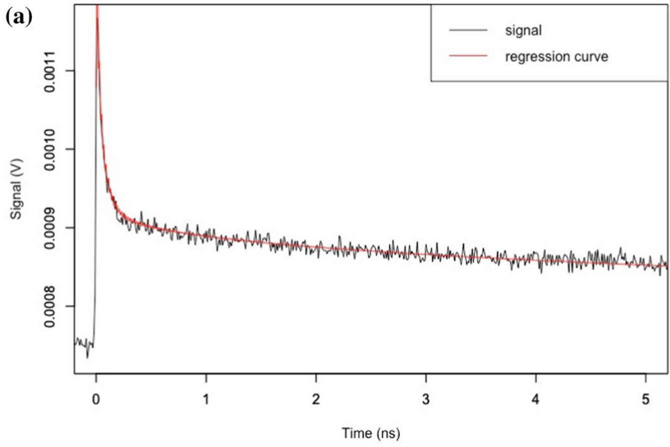
(a)
signal
regression curve
Signal (V)
0.0008
0.0009
0.0010
0.0011
0
1
2
3
4
5
Time (ns)

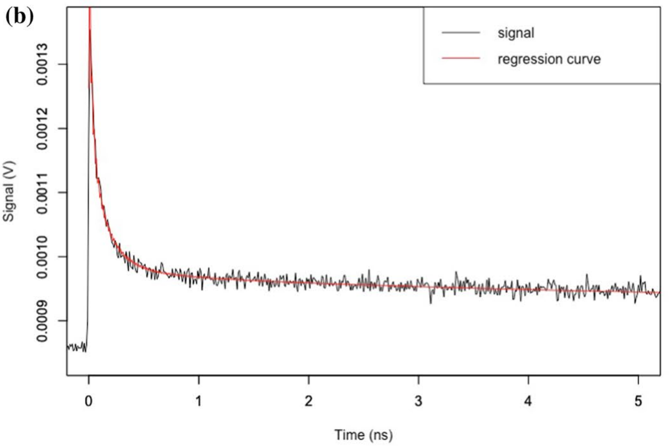
(b)
signal
regression curve
Signal (V)
0.0009
0.0010
0.0011
0.0012
0.0013
0
1
2
3
4
5
Time (ns)

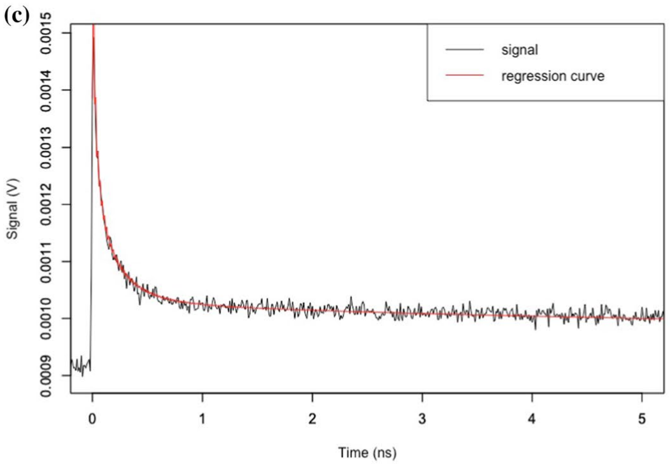
(c)
signal
regression curve
Signal (V)
0.0009
0.0010
0.0011
0.0012
0.0013
0.0014
0.0015
0
1
2
3
4
5
Time (ns)

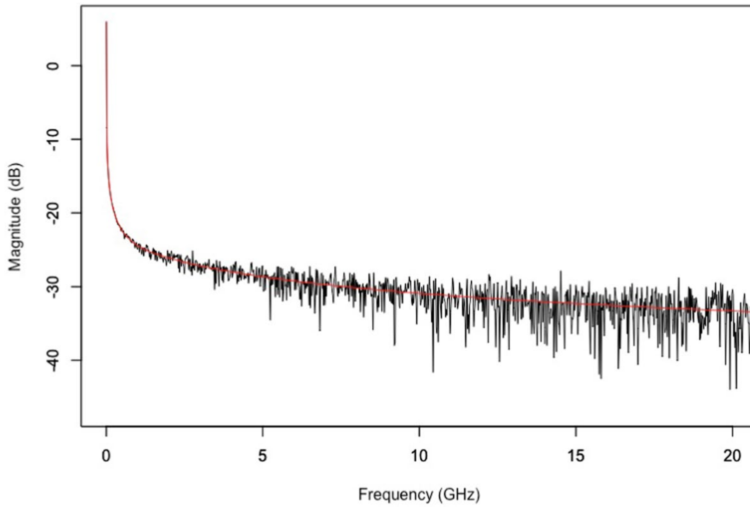

Fig. 4 Absolute of Fourier coefficients $|Y_n|$ of thermoreflectance signals obtained from the 100 nm thick Pt film and regression curves in frequency domain

Table 1 Estimates of fitting parameters and thermal properties determined by the parameters

d_f nm	$\hat{\tau}_f$ s	$\hat{\gamma}$	$\hat{\tau}_i$ s	α_f $m^2 \cdot s^{-1}$	l m
100	3.76×10^{-10}	0.708	2.00×10^{-11}	1.76×10^{-5}	1.87×10^{-8}
150	1.18×10^{-9}	0.729	1.55×10^{-11}	1.54×10^{-5}	1.55×10^{-8}
200	1.66×10^{-9}	0.683	1.26×10^{-11}	2.04×10^{-5}	1.60×10^{-8}

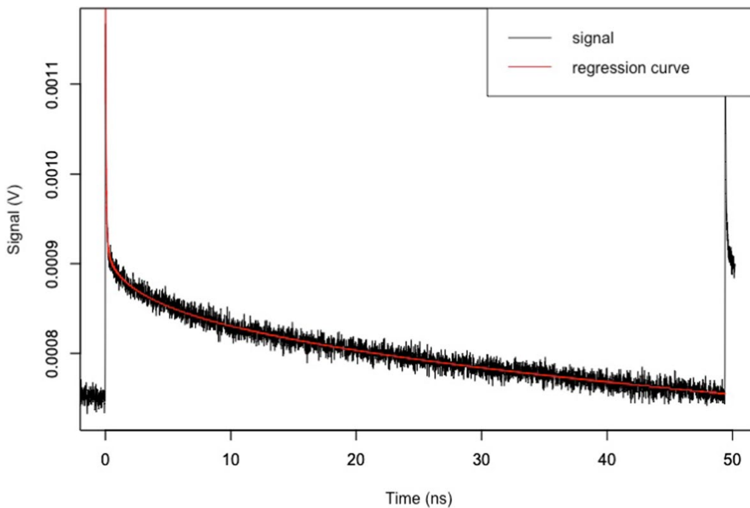

Fig. 5 Thermoreflectance signal under FF configuration from the 100 nm thick Pt film and regression curve in the whole observation time of 50 ns

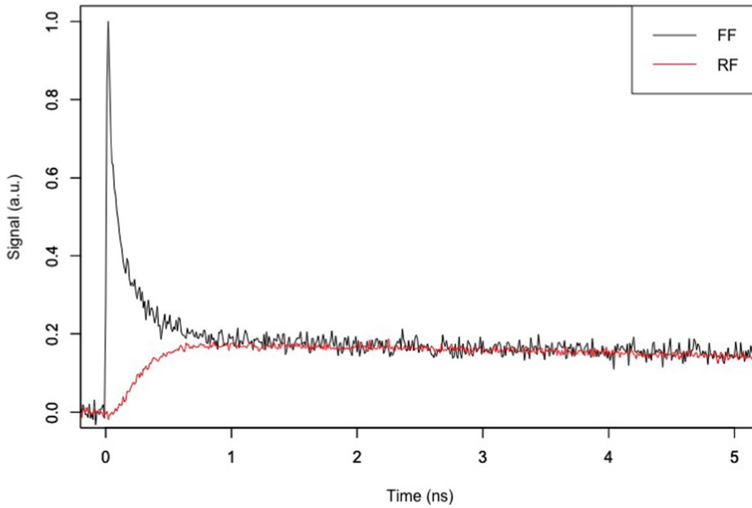

Fig. 6 Normalized thermoreflectance signals under FF and RF configuration from the 200 nm thick Pt film

Table 2 All the thermal diffusivity values obtained from the whole measurement

d_f nm		$\alpha_f/(\mathrm{m}^2/\mathrm{s})$					SD/Ave %
		1st	2nd	3rd	Average	SD	
100	FF	1.76×10^{-5}	2.03×10^{-5}	1.79×10^{-5}	1.86×10^{-5}	1.48×10^{-6}	7.96
	RF	1.54×10^{-5}	1.71×10^{-5}	1.72×10^{-5}	1.66×10^{-5}	1.01×10^{-6}	6.11
150	FF	1.54×10^{-5}	1.80×10^{-5}	1.78×10^{-5}	1.71×10^{-5}	1.45×10^{-6}	8.48
	RF	1.64×10^{-5}	1.63×10^{-5}	1.51×10^{-5}	1.59×10^{-5}	7.23×10^{-7}	4.54
200	FF	2.04×10^{-5}	2.28×10^{-5}	2.24×10^{-5}	2.19×10^{-5}	1.29×10^{-6}	5.88
	RF	1.91×10^{-5}	2.38×10^{-5}	2.52×10^{-5}	2.27×10^{-5}	3.20×10^{-6}	14.1

Table 3 All the penetration depth values obtained from the whole measurement

d_f nm	l/m					SD/Ave %
	1st	2nd	3rd	Average	SD	
100	1.87×10^{-8}	1.89×10^{-8}	1.85×10^{-8}	1.87×10^{-8}	2.00×10^{-10}	1.07
150	1.55×10^{-8}	1.60×10^{-8}	1.68×10^{-8}	1.61×10^{-8}	6.56×10^{-10}	4.07
200	1.60×10^{-8}	1.99×10^{-8}	1.84×10^{-8}	1.81×10^{-8}	1.97×10^{-9}	10.9

5 Discussion

In the conventional mathematical solution for FF configuration, which does not consider the penetration of pump beam, the temperature rise at 0 s is assumed to be

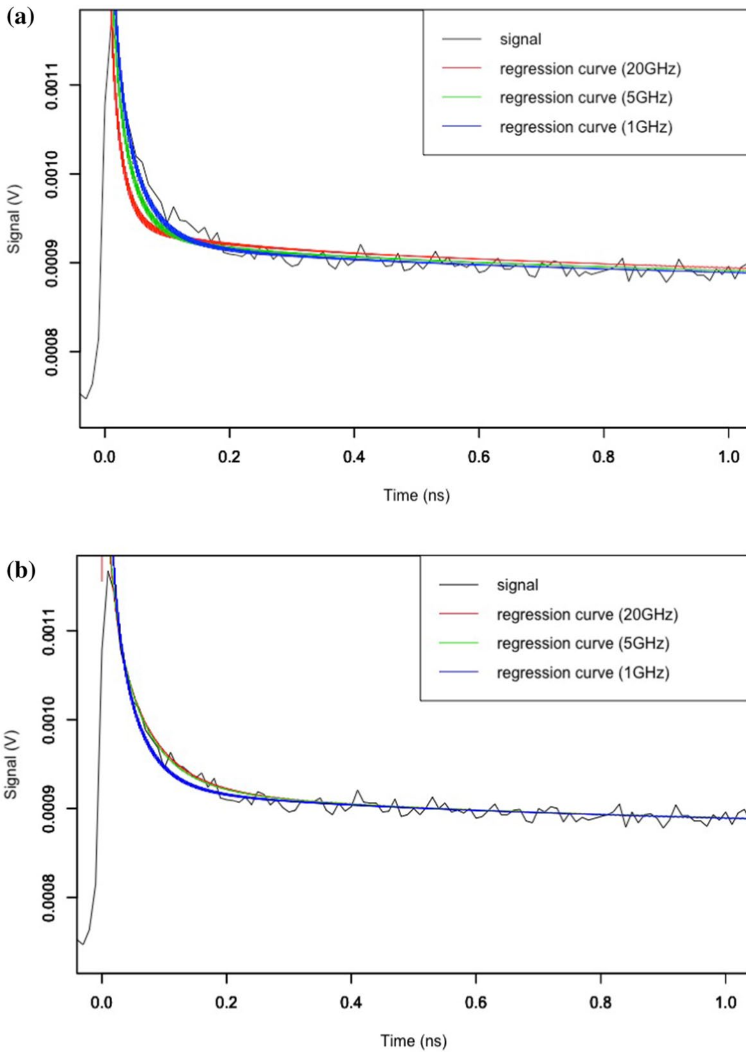

Fig. 7 (a): Regression curves in time domain from the conventional analytical solution (frequency components up to 20 GHz, 5 GHz, 1 GHz are considered). (b) Regression curves in time domain from the proposed analytical solution (frequency components up to 20 GHz, 5 GHz, 1 GHz are considered)

infinite, which is not the case of actual measurements.

Figure 7 shows the same thermoreflectance signals in Fig. 3(a). The red line, the green line, and the blue line in Fig. 7(a) are regression curves from the conventional analytical solution (τ_i is fixed at 0 in Eq. 28) when frequency components up to 20 GHz, 5 GHz, and 1 GHz are analyzed, by which thermal diffusivity of the thin film is determined at $5.67 \times 10^{-5}\ \mathrm{m}^2 \cdot \mathrm{s}^{-1}$, $3.68 \times 10^{-5}\ \mathrm{m}^2 \cdot \mathrm{s}^{-1}$, and $2.84 \times 10^{-5}\ \mathrm{m}^2 \cdot \mathrm{s}^{-1}$, respectively. Although the blue line is close to the observed thermoreflectance signal, the regression curve deviates from the signal as the upper

limit of frequency components increases from 1 to 20 GHz because the function $1/\sqrt{t}$ diverges at time $t = 0$.

On the other hand, the red line, the green line, and the blue line in Fig. 7(b) are the regression curves from the proposed analytical solution Eq. 28 when frequency components up to 20 GHz, 5 GHz, and 1 GHz are analyzed, by which thermal diffusivity of the thin film is determined at $1.76 \times 10^{-5}\ \mathrm{m^2 \cdot s^{-1}}$, $1.90 \times 10^{-5}\ \mathrm{m^2 \cdot s^{-1}}$, and $2.64 \times 10^{-5}\ \mathrm{m^2 \cdot s^{-1}}$, respectively. When the upper limit of frequency components increases from 1 to 20 GHz, the regression curve consistently fits the signal with small deviation. This robustness confirms the validity of the proposed analytical solution, which does not diverge but have finite value at $t = 0$. When the upper limit of frequency components is 1 GHz, the regression curve deviates from the signal at around 0.05 ns to 0.3 ns because of the lack of higher frequency components.

6 Conclusion

We have derived a new analytical formula which considers the penetration of pump beam and probe beam in thermoreflectance method under FF configuration. We measured three Pt thin film with different thickness (100 nm, 150 nm, and 200 nm) deposited on fused quartz substrate both under FF and RF configuration. By applying Fourier expansion analysis and the new formula which considers the penetration depth of beam to the thermoreflectance signals, consistent thermal diffusivity values were obtained from both FF and RF configuration, which agree within deviation smaller than 10 % for 150 nm thick and 200 nm thick Pt thin film. Our new approach realized the quantitative determination of thermal diffusivity of metallic thin films located in first layer under FF configuration, which has been a long-term unsolved issue in this field for more than 35 years. In future, we would like to extend our analytical approach to more complicated models like multi-layer models.

Appendix

When pump beam and probe beam are incident on a thin film, the beams penetrate a finite length from the surface, as shown in Fig. 8, in the case of FF configuration. Since the heated face can be assumed to be adiabatic to the environment in the observation period of 50 ns, contribution of the mirror image of the pulse heating should be added to the temperature response. The temperature rise after light heating with a single pulse $T_{obs}(t)$ is represented by the dual convolution of an infinite series of Green's function with heating distribution function for the penetration depth of pump beam δ_h, and the penetration depth of probe beam δ_d, by the following equation.

$$T_{obs}(t) = T_{real}(t) + T_{mirror}(t), \tag{34}$$

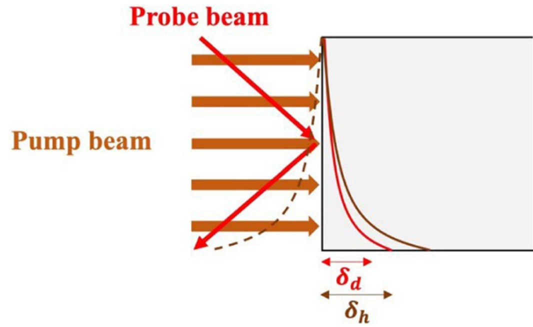

Fig. 8 Schematic diagram of penetration of pump beam and probe beam

where T_{real} is temperature rise by real heat source and T_{mirror} is temperature rise by the mirror image heat source.

The contribution from the real heat source is calculated as follows.

$$T_{real}(t) = \frac{1}{2b\sqrt{\pi t}}\int_0^\infty\int_0^\infty D(x_d)\exp\left(-\frac{(x_d-\chi_h)^2}{4\alpha t}\right)Q(\chi_h)d\chi_h\, dx_d \quad (35)$$

$$D(x_d) = \frac{1}{\delta_d}\exp\left(-\frac{x_d}{\delta_d}\right) \quad (36)$$

$$Q(x_h) = \frac{1}{\delta_h}\exp\left(-\frac{\chi_h}{\delta_h}\right) \quad (37)$$

Equation 35 can be analytically solved by coordinate conversion and using the Jacobian determinant as expressed by the following equations.

$$x_d + \chi_h = \eta \quad (38)$$

$$x_d - \chi_h = \mu \quad (39)$$

$$dx_d d\chi_h = \left(\frac{dx_d}{d\eta}\frac{d\chi_h}{d\mu} - \frac{dx_d}{d\mu}\frac{d\chi_h}{d\eta}\right)d\eta d\mu = \frac{1}{2}d\eta d\mu \quad (40)$$

Then, Eq. 35 is transformed to the following equation.

$$T_{real}(t) = \frac{1}{4\delta_d\delta_h b\sqrt{\pi t}}\int_0^\infty\int_{-\eta}^{\eta}\exp\left(-\frac{1}{2}\left(\frac{1}{\delta_d}+\frac{1}{\delta_h}\right)\eta\right)\exp\left(-\frac{\mu^2}{4\alpha t}\right)\exp\left(-\frac{1}{2}\left(\frac{1}{\delta_d}-\frac{1}{\delta_h}\right)\mu\right)d\mu d\eta \quad (41)$$

To simplify the equation, the following parameters are defined.

$$\kappa_+ = \frac{1}{2}\left(\frac{1}{\delta_d}+\frac{1}{\delta_h}\right) \quad (42)$$

$$\kappa_{-} = \frac{1}{2}\left(\frac{1}{\delta_d} - \frac{1}{\delta_h}\right) \tag{43}$$

Then, Eq. 41 is transformed to the following equation.

$$T_{real}(t) = \frac{1}{4\delta_d\delta_h b\sqrt{\pi t}}\int_0^{\infty}\exp\left(-\kappa_{+}\eta\right)\int_{-\eta}^{\eta}\exp\left(-\kappa_{-}\mu\right)\exp\left(-\frac{\mu^2}{4\alpha t}\right)d\mu d\eta \tag{44}$$

This equation can be integrated by parts as follows

$$\begin{aligned} T_{real}(t) = & \frac{1}{4\delta_d\delta_h b\sqrt{\pi t}}\left[\frac{\exp\left(-\kappa_{+}\eta\right)}{-\kappa_{+}}\int_{-\eta}^{\eta}\exp\left(-\kappa_{-}\mu\right)\exp\left(-\frac{\mu^2}{4\alpha t}\right)d\mu\right]_0^{\infty} \\ & - \frac{1}{4\delta_d\delta_h b\sqrt{\pi t}}\int_0^{\infty}\frac{\exp\left(-\kappa_{+}\eta\right)}{-\kappa_{+}}\left(\exp\left(-\kappa_{-}\eta\right)\exp\left(-\frac{\eta^2}{4\alpha t}\right)\right. \\ & \left. +\exp\left(\kappa_{-}\eta\right)\exp\left(-\frac{\eta^2}{4\alpha t}\right)\right)d\eta \end{aligned} \tag{45}$$

The following equation with complementary error functions is finally derived from Eq. 45.

$$T_{real}(t) = \frac{1}{\sqrt{\pi}c\rho\left(\delta_d+\delta_h\right)}\left(\exp\left(\frac{t}{\tau_d}\right)\mathrm{erfc}\left(\sqrt{\frac{t}{\tau_d}}\right) + \exp\left(\frac{t}{\tau_h}\right)\mathrm{erfc}\left(\sqrt{\frac{t}{\tau_h}}\right)\right) \tag{46}$$

$$\tau_d = \frac{{\delta_d}^2}{\alpha} \tag{47}$$

$$\tau_h = \frac{{\delta_h}^2}{\alpha}, \tag{48}$$

where τ_d is heat diffusion time across the penetration depth of probe beam and τ_h is heat diffusion time across the penetration depth of pump beam. Since distance between the mirror image heat source and the detection point is

$x_d + \chi_h(= \eta)$, the contribution from the mirror image heat source is calculated as follows.

$$T_{mirror}(t) = \frac{1}{2b\sqrt{\pi t}}\int_0^{\infty}\int_0^{\infty}D\left(x_d\right)\exp\left(-\frac{\left(x_d + \chi_h\right)^2}{4\alpha t}\right)Q\left(\chi_h\right)d\chi_h\, dx_d \tag{49}$$

The following equation is derived from Eq. 49 in a similar way.

$$T_{mirror}(t) = \frac{1}{\sqrt{\pi}c\rho\left(\delta_d-\delta_h\right)}\left(\exp\left(\frac{t}{\tau_d}\right)\mathrm{erfc}\left(\sqrt{\frac{t}{\tau_d}}\right) - \exp\left(\frac{t}{\tau_h}\right)\mathrm{erfc}\left(\sqrt{\frac{t}{\tau_h}}\right)\right) \tag{50}$$

According to Eq. 34, the net temperature rise $T_{obs}(t)$ is finally expressed as follows.

$$T_{obs}(t) = \frac{2}{\sqrt{\pi}c\rho}\left(\frac{\delta_d}{{\delta_d}^2 - {\delta_h}^2}\exp\left(\frac{t}{\tau_d}\right)\mathrm{erfc}\left(\sqrt{\frac{t}{\tau_d}}\right) - \frac{\delta_h}{{\delta_d}^2 - {\delta_h}^2}\exp\left(\frac{t}{\tau_h}\right)\mathrm{erfc}\left(\sqrt{\frac{t}{\tau_h}}\right)\right) \tag{51}$$

When either δ_d or δ_h is 0, the equation converges to the equation where only the penetration of pump beam or only the penetration of probe beam is considered, respectively. When δ_d and δ_h are equal, the equation converges to the single equation with single diffusion time $\tau_p(= \tau_h= \tau_d)$. The numerator of 2 in Eq. 51 is a coefficient due to the addition of the mirror image heat source.

Acknowledgments Takahiro Baba and Tetsuya Baba would like to thank Dr. Naoyuki Taketoshi and Dr. Takashi Yagi of the National Metrology Institute of Japan, the National Institute of Advanced Industrial Science and Technology for information about picosecond thermoreflectance technology using mode-lock fiber lasers.

Author Contributions T.B.(Takahiro Baba) contributed toward methodology, analysis, investigation, and writing. T.B.(Tetsuya Baba) contributed toward conceptualization, review and editing, and supervision. T.M.(Takao Mori) contributed toward conceptualization, review and editing, supervision, and funding acquisition

Funding The authors acknowledge support from JST Mirai Program Grant Number JPMJMI19A1. Takahiro Baba was also supported by JST SPRING, Grant Number JPMJSP2124.

Data Availability The data that support the findings of this study are available from the corresponding author upon reasonable request.

Declarations

Conflict of interest One Japanese patent application (Appl. No. 2018-516599, Patent No. 6399329), one PCT patent application (PCT/JP2018/012324), and one United States patent application (16/620.294) related to the work described here.

Open Access This article is licensed under a Creative Commons Attribution 4.0 International License, which permits use, sharing, adaptation, distribution and reproduction in any medium or format, as long as you give appropriate credit to the original author(s) and the source, provide a link to the Creative Commons licence, and indicate if changes were made. The images or other third party material in this article are included in the article's Creative Commons licence, unless indicated otherwise in a credit line to the material. If material is not included in the article's Creative Commons licence and your intended use is not permitted by statutory regulation or exceeds the permitted use, you will need to obtain permission directly from the copyright holder. To view a copy of this licence, visit http://creativecommons.org/licenses/by/4.0/.

References

1. D.G. Cahill, Microscale Thermophys. Eng. **1**, 85–109 (1997)
2. Special Issue: Thermal Design and Thermophysical Property for Electronics: Jpn. J. Appl. Phys. **48**, 5S2 (2009).
3. Special Issue: Thermal Design and Thermophysical Property for Electronics and Energy: Jpn. J. Appl. Phys. **50**, 11S (2011).
4. D.G. Cahill, K.E. Goodson, A. Majumdar, J. Heat Transf. **124**, 223 (2002)

5. D.G. Cahill, W.K. Ford, K.E. Goodson, G.D. Mahan, A. Majumdar, H.J. Maris, R. Merlin, S.R. Phillpot, Appl. Phys. Lett. **93**, 793 (2003)
6. T. Nakai, S. Ashida, K. Todori, K. Yusu, K. Ichihara, S. Tatsuta, N. Taketoshi, T. Baba, Opt. Data Storage **2004**, 464–473 (2004)
7. X. Chen, Z. Zhou, Y.H. Lin, C. Nan, J. Mater. **6**, 494–512 (2020)
8. T. Hendricks, T. Caillat, T. Mori, Energies **15**, 7307 (2022)
9. C.A. Paddock, G.L. Eesley, J. Appl. Phys. **60**, 285–290 (1986)
10. A. Rosencwaig, J. Ospal, W. Smith, D. Willenborg, Appl. Phys. Lett. **46**, 1013–1015 (1985)
11. N. Taketoshi, T. Baba, A. Ono, High Temp. High Press. **29**, 59–66 (1997)
12. T. Baba, N. Taketoshi, Proc. Eurotherm 57 Poitiers, 31, 285–292 (1999)
13. N. Taketoshi, T. Baba, A. Ono, *Thermal Conductivity 24* (Technomic Publishing, Lancaster, 1999), pp.289–302
14. W.J. Parker, R.J. Jenkins, C.P. Butler, G.L. Abbott, J. Appl. Phys. **32**, 1679 (1961)
15. F. Righini, A. Cezairliyan, High Temp. High Press. **5**, 481 (1973)
16. A. Cezairliyan, T. Baba, R. Taylor, Int. J. Thermophys. **15**, 317–341 (1994)
17. T. Baba, A. Ono, Meas. Sci. Technol. **12**, 2046–2057 (2001)
18. N. Taketoshi, T. Baba, A. Ono, High Temp. High Press. **34**, 19–28 (2002)
19. K. Kobayashi, T. Baba, Jpn. J. Appl. Phys. **48**, 05EB05 (2009)
20. N. Taketoshi, T. Baba, A. Ono, Jpn. J. Appl. Phys. **38**, L1268 (1999)
21. N. Taketoshi, T. Baba, A. Ono, Meas. Sci. Technol. **12**, 2064 (2001)
22. T. Yagi, K. Tamano, Y. Sato, N. Taketoshi, T. Baba, Y. Shigesato, J. Vac. Sci. Technol. A **23**, 1180 (2005)
23. T. Baba, N. Taketoshi, T. Yagi, Jpn. J. Appl. Phys. **50**, 11RA01 (2011)
24. R.M. Costescu, M.A. Wall, D.G. Cahill, Phys. Rev. B **67**, 054302 (2003)
25. H.K. Lyeo, D.G. Cahill, Phys. Rev. B **73**, 144301 (2006)
26. P. Jiang, X. Qian, R. Yang, J. Appl. Phys. **124**, 161103 (2018)
27. P.E. Hopkins, R.N. Salaway, R.J. Stevens, P.M. Norris, Int. J. Thermophys. **28**, 947–957 (2007)
28. F. Sun, X. Wang, M. Yang, Z. Chen, H. Zhang, D. Tang, Int. J. Thermophys. **39**, 5 (2018)
29. N. Taketoshi, T. Baba, A. Ono, Rev. Sci. Instrum. **76**, 094903 (2005)
30. Y. Isosaki, Y. Yamashita, T. Yagi, J. Jia, N. Taketoshi, S. Nakamura, Y. Shigesato, J. Vac. Sci. Technol. A **35**, 041507 (2017)
31. Y. Yamashita, K. Honda, T. Yagi, J. Jia, N. Taketoshi, Y. Shigesato, J. Appl. Phys. **125**, 035101 (2019)
32. T. Baba, T. Baba, K. Ishikawa, T. Mori, J. Appl. Phys. **130**, 225107 (2021)
33. T. Baba, T. Baba, T. Mori, Int. J. Thermophys. **45**, 27 (2024)
34. T. Baba, Jpn. J. Appl. Phys. **48**, 05EB04 (2009)
35. J.R. Rumble, *CRC Handbook of Chemistry and Physics*, 99th edn. (CRC Press, LLC, Boca Raton, 2018)

Publisher's Note Springer Nature remains neutral with regard to jurisdictional claims in published maps and institutional affiliations.